Microelectronic Engineering 194 (2018) 45–50

Contents lists available at ScienceDirect

Microelectronic Engineering

journal homepage: www.elsevier.com/locate/mee

Research paper

Improved development procedure to enhance the stability of microstructures created by two-photon polymerization

Julia Purtov[a,b], Andreas Verch[a], Peter Rogin[a], René Hensel[a,*]

[a] INM – Leibniz Institute for New Materials, Campus D2 2, Saarbrücken 66123, Germany
[b] Department of Materials Science and Engineering, Saarland University, Campus D2 2, 66123 Saarbrücken, Germany

ARTICLE INFO

Keywords:
Two-photon polymerization
Microstructures
Development

ABSTRACT

Natural functional surfaces often rely on unique nano- and micropatterns. To mimic such surfaces successfully, patterning techniques are required that enable the fabrication of three-dimensional structures at the nanoscale. It has been reported that two-photon polymerization (TPP) is a suitable method for this. However, polymer structures fabricated by TPP often tend to shrink and to collapse during the fabrication process. In particular, delicate structures suffer from their insufficient mechanical stability against capillary forces which mainly arise in the fabrication process during the evaporation of the developer and rinsing liquids. Here, we report a modified development approach, which enables an additional UV-treatment to post cross-link created structures before they are dried. We tested our approach on nanopillar arrays and microscopic pillar structures mimicking the moth-eye and the gecko adhesives, respectively. Our results indicate a significant improvement of the mechanical stability of the polymer structures, resulting in fewer defects and reduced shrinkage of the structures.

1. Introduction

In the last decade, two-photon polymerization (TPP) has been established as a versatile tool for the microfabrication of complex, three-dimensional structures [1]. Applications include the fabrication of photonic crystals [2], directly printed lens systems [3], microfluidic devices [4], biological scaffolds [5], and templates for metamaterials [6,7]. In general, TPP relies on similar principles as known for common optical lithography, namely, exposure of an often negative photo-resist and a wet development process followed by the drying of the structures. In contrast to classic optical lithography, TPP uses a focused, femtosecond-pulsed, near-infrared (NIR) laser allowing highly controlled spatial two-photon polymerization [8]. The size of the reaction volume, the so-called voxel, determines the resolution of the system, which is typically in the range of a few hundreds of nanometers [9,10]. By stacking voxels in all dimensions various three-dimensional (3d) structures can be fabricated.

Despite the opportunity to generate high resolution 3d structures, TPP bears several obstacles. One of the biggest challenges is the discrepancy between the dimensions of the designed 3d model and the final polymer structure [11–13]. The reasons for that are defects caused by surface wrinkling, strong and anisotropic shrinkage of the polymer, and the collapse of structural features due to insufficient mechanical stability. In order to at least mitigate these failures, several approaches have been discussed [14–16]. It has been proposed to modify the 3d model to compensate for the expected shrinkage [14], or to add so called shrinkage guides to the original design to achieve isotropic shrinkage [15]. The cross-linking density of the resist, and therefore its mechanical stability, can be improved by longer laser exposure times [16]. This, though, leads inevitably to increased feature sizes. In addition to shrinkage driven effects, capillary forces can cause significant defects, such as deformation or collapse of structures. Capillary forces usually occur during drying, i.e. the evaporation of the rinsing solution during the last process step. In order to reduce capillary forces liquids with low surface tension [17,18], for example hexamethyldisilazane, or critical point drying [19,20] are used. However, these approaches contain several process steps and, therefore, are more time consuming.

In this paper, we report a modified development protocol for TPP to produce nano- and microscopic structures with enhanced mechanical stability, reduced material shrinkage and fewer defects. In the new development procedure, the specimens were kept immersed in developer and rinsing liquids until the structures were mechanically stabilized by an additional ultraviolet (UV) exposure. It is anticipated, that the UV-exposure provides further cross-linking between the reactive sites of the resist molecules, which remained unreacted after the initial laser exposition. As a result, the stability of the structure enhances and becomes more resistant against capillary forces. The new approach is demonstrated on nanopillar arrays as well as microstructures, and is

* Corresponding author.
E-mail address: rene.hensel@leibniz-inm.de (R. Hensel).

https://doi.org/10.1016/j.mee.2018.03.009
Received 20 December 2017; Received in revised form 25 February 2018; Accepted 12 March 2018
Available online 13 March 2018

compared to the same motives developed by the conventional procedure without the additional UV-treatment. Created nanopillar arrays were inspired by structures found on the moth's eye [21–23], while the micropillars with mushroom-shaped tips mimicked the adhesive gecko toes [24,25]. The results obtained demonstrate that an additional cross-linking step during the development enhances the stability of TPP-structures and helps to reduce defects and material shrinkage. By this, the proposed approach offers high potential for a reliable fabrication of high-resolution structures and is easily integrated into existing process schemes.

2. Experimental

2.1. Two-photon patterning

Nanopillar structures were defined using the DeScribe-software of the two-photon polymerization (TPP) system (Professional GT, Nanoscribe, Germany). These pillars were arranged in 50 × 50 μm arrays with pitch distances ranging from 280 nm up to 1700 nm. In contrast, the 3d-design for gecko-inspired microstructures was created using a computer assisted design (CAD) software (Inventor, Autodesk, USA). All structures were fabricated from a negative photo resist (IP-Dip, Nanoscribe, Germany) on fused silica substrates. For the microstructures, (3-methacryloyloxypropyl) trichlorosilane (Abcr, Germany) was immobilized on the substrates via vapor deposition to enhance the adhesion of the acryl-based resist to the substrate [26]. The structures were generated using the so-called “dip-in mode” where the objective of the TPP-System (63× with NA = 1.4, Zeiss, Germany) is dipped directly into the resist. Exposure parameters were 25 mW and 50.000 μm/s for laser power and scan speed, respectively.

2.2. Development procedures

Following the conventional development process (see black route in Fig. 1), the structures were developed by immersion into propylene glycol monomethyl ether acetate (PGMEA, Sigma Aldrich, Germany) for 20 min at room temperature to remove unbound monomeric material. After that, the structures were carefully rinsed using isopropanol (IPA, Sigma Aldrich, Germany) and subsequently dried in air by evaporation.

Following the development proposed in this study (see red route in Fig. 1), after the 20 min of development 70% of the PGMEA were carefully replaced with isopropanol without exposing the structures to air. This solvent exchange was repeated three times, separated by a residence time of 10 min. In contrast to the conventional method, the specimens were additionally cross-linked using UV-exposure for 300 s (200 W, OmniCure S1500A, igb-tech, Germany), while the samples were still immersed in isopropanol. The UV source had a maximum peak at 365 nm (see Fig. S1 in the Supporting information) and an intensity of 51 mW/cm^2. Finally, the samples were removed from the liquid, rinsed with fresh isopropanol, and dried in air.

2.3. Scanning electron microscopy

Scanning electron micrographs of generated TPP-structures were examined at tilt angles of 0°, 40° and 50° in high-vacuum mode using a Quanta 250 FEG (FEI, The Netherlands) equipped with an Everhart-Thornley-detector (ETD). The spot size and the accelerating voltage were set to 2.0 and 2 kV, respectively. Samples were fixed with clamps on a metallic sample holder. A copper tape was placed close to the samples to minimize charging effects. The specimens were not coated with conductive material to maintain their optical properties. The ratios between upright and collapsed pillars were determined by analyzing scanning electron micrographs at lower magnification showing whole nanopillar arrays at 0° incident angle. Shrinkage of TPP-structures was evaluated on micropillars by measuring the pillar heights, pillar diameters, the diameter of the disc, and the diameter at the pillar-substrate-interface.

2.4. Optical properties

The optical characteristics of the nanopillar arrays were extracted from optical microscopy images recorded with an Eclipse LV100ND (Nikon, Japan) equipped with a 20× color-corrected objective. The microscope was operated in the bright field mode with a fully opened aperture. Prior to examination, white balance was set using a white sheet of paper.

3. Results

The main idea of the new development procedure, as described in Section 2.2 and as illustrated in Fig. 1, is to provide additional stabilization to the structural features before exposing them to capillary forces. This was exemplified on nanoscopic and microscopic pillar arrays, respectively.

3.1. Nanopillar arrays

Two identical specimens were created by TPP comprising a series of 50 × 50 μm arrays of nanopillar structures with varying pitch distances, p, from 280 to 1700 nm. The pitch distance specifies the distance between adjacent pillars (see Fig. 6b). One specimen was developed according to the conventional, the other according to the improved development strategy introduced in Fig. 1. The structures obtained were investigated using SEM and fractions of upright standing and collapsed pillars were determined. The optical properties of whole arrays were analyzed using optical microscopy.

The resulting nanopillar arrays and the fractions of free standing pillars are presented in Figs. 2 and 3. The conventionally developed array with $p = 1700$ nm exhibited 54% upright standing pillars, whereas 46% of the pillars were collapsed or detached from the substrate during the development (Fig. 3). The pillar heights and diameters (Fig. 2a) were 1050 ± 31 nm and 326 ± 8 nm, respectively. Most free ends of the pillar structures were slightly bent. Similar results were obtained for pitch distances of 1560 nm, 1420 nm, and 1270 nm. For smaller pitch distances, the bending of the free ends of the nanopillars was more prominent. At a pitch distance of 1130 nm, structures condensed into aggregates. As a consequence, the fraction of upright pillars drastically dropped to 15%. With further decreasing pitch, the number of pillars forming aggregates increased. At a pitch distance of 710 nm, all individual pillars were integrated into aggregates and no upright standing pillars were observed. At the smallest pitch distance of 280 nm, the spacing between pillars was smaller than the diameter of the voxels. Hence, the pillar structures laterally overlapped and formed a rough quasi-film without any recognizable pillar structures.

For the nanopillar arrays developed by the improved development procedure, scanning electron micrographs revealed the same pillar sizes as reported for the conventional development above. However, most of the pillars stayed upright and had straight tips (Fig. 2d). 100% upright standing pillars without any tip bending were obtained for all pitch distances down to 570 nm (Fig. 3). At a pitch distance of 420 nm, the fraction of upright pillars was still almost 100%, but a slight bending of the structures and pillar agglomeration occurred. Similar to the conventionally created pillar arrays, the structures fused into a rough quasi-film at the smallest pitch distance.

The optical analysis revealed a strong correlation between the homogeneity in the optical appearance of arrays and the fraction of upright pillars. The conventionally developed arrays appeared slightly colored in regions with upright standing pillars and colorless in regions where pillars were missing or had collapsed (Fig. 2b). In contrast, arrays developed with the improved approach appeared more saturated in color, particularly for pitch spacings in the range between 570 and

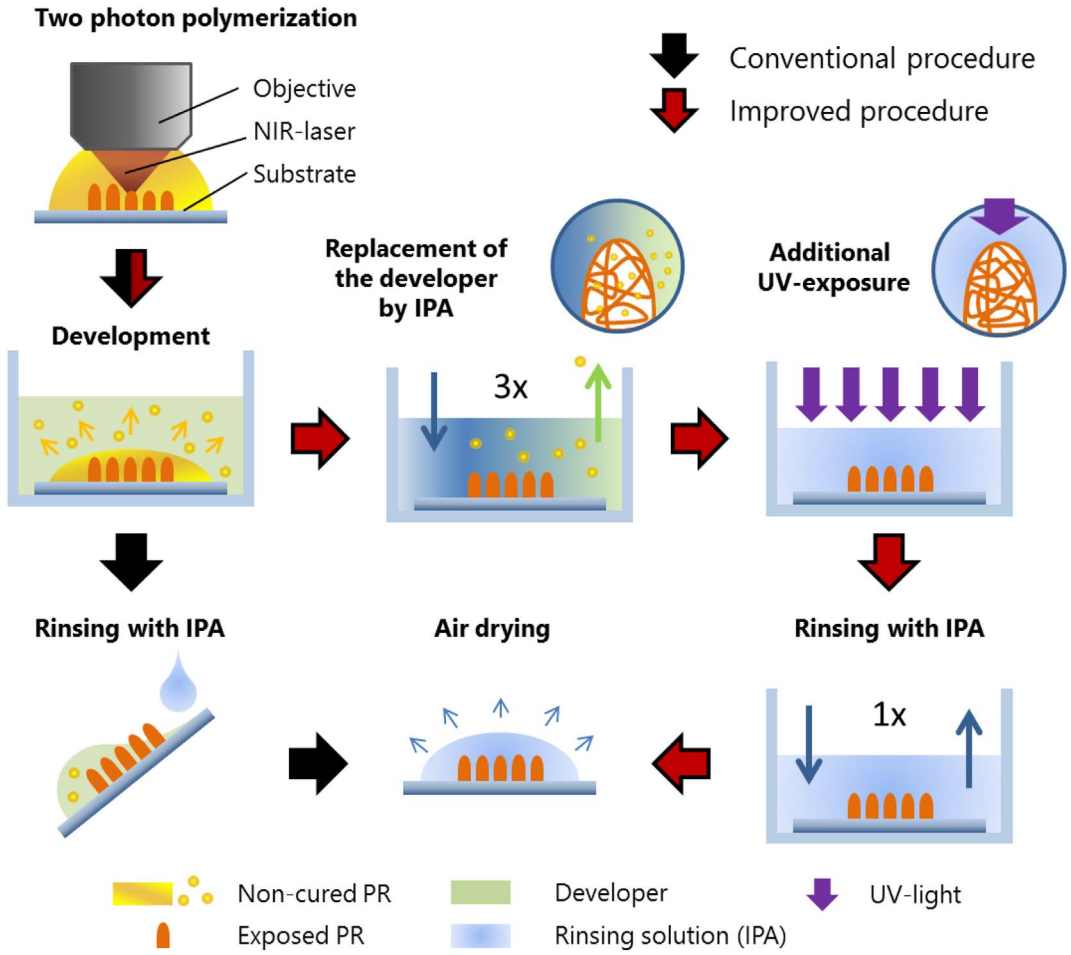

Fig. 1. Schematic illustration of the conventional and the improved wet development approach. Upon two-photon polymerization via near-infrared (NIR)-laser exposure, the structures are developed to remove unexposed photo-resist (PR). The conventional development (black arrows) includes the development in the developer liquid followed by careful rinsing with isopropanol (IPA) and drying of the specimen. The improved proposed procedure (red arrows) includes gentle replacement of the developer-monomer-mixture with isopropanol, while structures are kept immersed during the whole procedure. Next, the structures are further cross-linked by additional ultra violet (UV) exposure. Finally, the structures are rinsed and dried in air. (For interpretation of the references to color in this figure legend, the reader is referred to the web version of this article.)

990 nm (Fig. 2c). None of these arrays exhibited colorless areas due to pillar collapses and therefore gave a homogeneous optical impression.

3.2. Microscopic structures

Microscopic mushroom-shaped pillars were created based on a CAD model. The model used, and the resulting microscopic pillar arrays developed by both, the conventional and the improved development approach are displayed in Fig. 4. The model consisted of a cylindrical pillar with straight side walls and a disc at the free end forming the so-called mushroom tip (Fig. 4a). The conventionally developed structures were strongly deformed and exhibited collapsed parts (Fig. 4b). In contrast, the structures obtained upon the improved approach exhibited straight sidewalls and a smooth top disc, close to the computer model. Only a surface roughness at the sidewalls originating from the writing process (i.e., the vertical stacking of slices) was observed. Fig. 5 shows an analysis of the shrinkage by comparing the originally defined dimensions in the 3d CAD-model with the real dimensions determined for fabricated structures. The pillars were designed with a diameter of 24 µm and a height of 39.5 µm. A disc with 30 µm diameter and 0.5 µm thickness represented the mushroom tip. For the conventional development, about 20% shrinkage in the pillar height and the disc diameter were observed. The pillar diameter shrunk by 26%. Even at the pillar-substrate interface, 8% shrinkage was found. For the structures developed with the improved method, an overall shrinkage of about 10% for the pillar height, pillar diameter, as well as the disc diameter were obtained. The shrinkage at the pillar-substrate interface was negligible.

4. Discussion

In this work, we propose a novel development approach for two-photon polymerization that, in particularly, facilitates the creation of closely packed nanopillar arrays and complexly shaped microscopic structures.

In fact, the collapse of densely packed nanostructures could be prevented down to a pitch distance, p, of 420 nm, whereas conventionally developed pillars collapsed already at the much larger pitch distance of 1130 nm. In general, two different types of pillar collapse can be distinguished: on the one hand the ground collapse, that is pillars detach from the substrate when the spacing between adjacent pillars is larger than the height of the pillars [12], on the other hand the lateral collapse, that is pillars cluster or form agglomerates when the spacing between pillars is smaller than their height [27]. For the structures developed with the conventional method, we observed ground collapse at $p = 1420$ nm and three different degrees of lateral collapse depending on the pitch distance (Fig. 6a): upright pillars with bent tips ($p = 1130$ nm), pairs of attached pillars ($p = 990$ nm) and clusters of more than two pillars ($p < 850$ nm).

The collapse of the nanopillar arrays is most likely induced by capillary forces. These forces act at each individual pillar tip at the three-

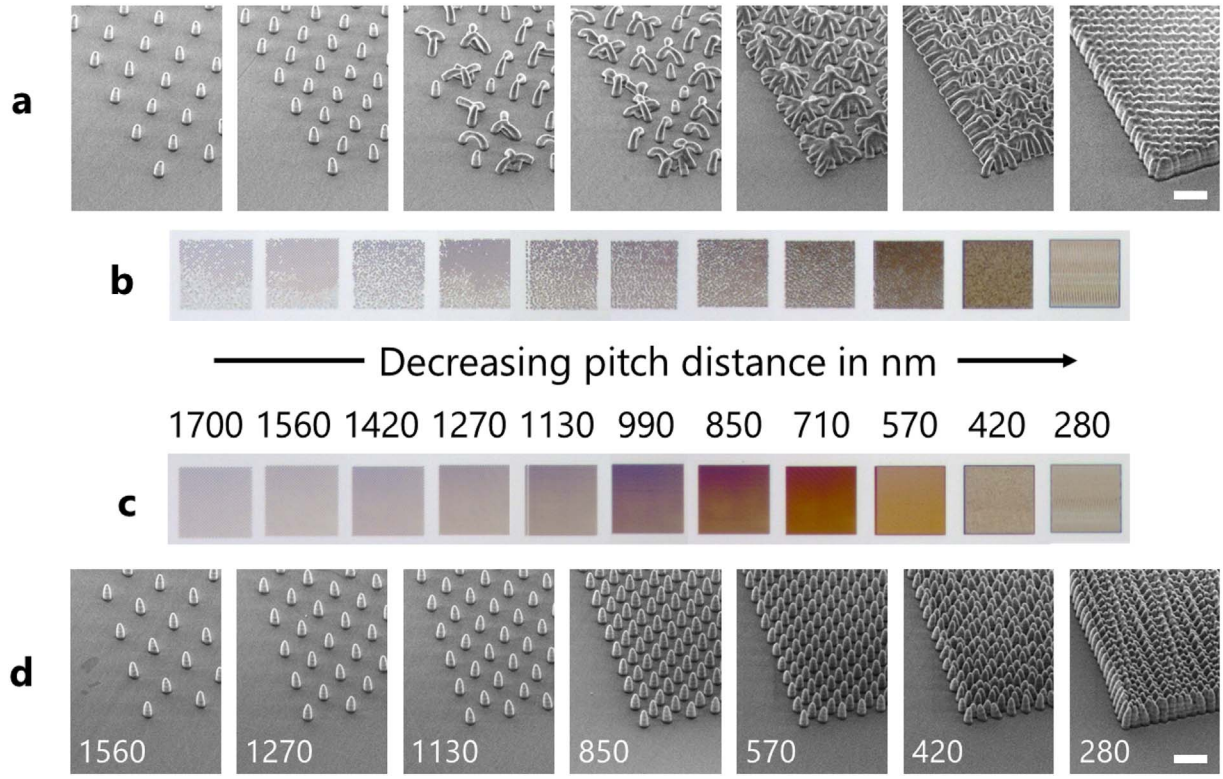

Fig. 2. Nanopillar arrays with different pitch distances developed (a,b) by the conventional and (c,d) by the improved strategy. (a,d) Scanning electron images of pillar arrays at 40° tilt; the scale bar is 2 µm. (b,c) Bright field optical micrographs of 50 × 50 µm nanopillar arrays on a fused silica substrate.

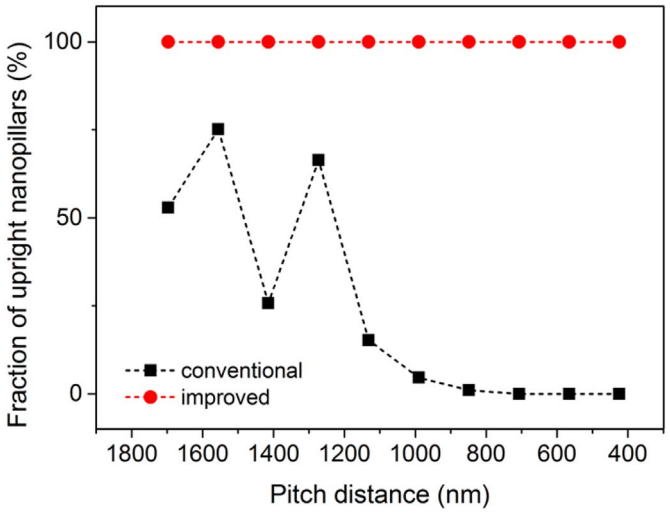

Fig. 3. Fraction of upright nanopillars as a function of the pitch distance. The fraction of upright nanopillars is the number of upright standing pillars, i.e. pillars showing no collapse or agglomeration, normalized to the total number of pillars per array. Red circles represent the results of arrays developed by the improved development procedure including post UV exposure. Black squares depict the results of arrays developed using the conventional development approach. Dashed lines are intended to guide the eye. (For interpretation of the references to color in this figure legend, the reader is referred to the web version of this article.)

phase contact line during the drying of the structures (Fig. 6b) [28,29]. The capillary force is given by $F_C = (2\pi\gamma r^2/(p - 2\delta))cos^2\theta$, where γ is the surface tension of the liquid, here isopropanol, r is the radius of the pillars, θ is the receding contact angle, and δ denotes the deflection of the pillar [25]. The term $(p - 2\delta)$ reflects the actual spacing between two pillar tips, which dynamically changes when the pillars bend [29]. In the undeformed state, when $\delta = 0$, the force is the higher the denser the array is packed, because F_C scales inversely proportional to p. The capillary force increases with increasing δ and is highest just before two adjacent pillars touch each other. At this point, δ equals approximately $p/2$. An elastic restoring force, F_E, is acting against the described bending induced by the capillary forces and is given by $F_E = 3\pi Er^4\ \delta/4h^3$, where E is Young's modulus and h the height of the pillars [25]. The elastic restoring force increases linearly with δ. If F_E is larger than F_C, the pillars will resist capillary forces and the fraction of upright pillars in the dried array will be high. In contrast, if F_E is smaller than F_C, the pillars will most likely bend and collapse. After the liquid is evaporated completely, mainly van der Waals forces, F_{vdW}, act between attached pillars. Hence, the stability of agglomerates formed by capillarity depends on the force balance between F_E and F_{vdW} [29]. For $F_E > F_{vdW}$, the pillars most likely snap back to a vertical position, but a slight bending of the tips can be maintained due to plastic deformations. For $F_E < F_{vdW}$, the pillars remain in contact at the tips. With decreasing spacing between the pillars, the maximum deflection of the pillars decreases, hence F_E decreases and, therefore, the probability for the formation of agglomerates increases. This is in line with our observations shown in Fig. 2. However, the smallest pitch allowing intact, upright standing pillar arrays, varied with the development procedure. Most likely, the additional UV-treatment during the improved procedure facilitated an elevated cross-linking density, which is associated with an increased Young's modulus. As the elastic restoring force scales linearly with Young's modulus, the mechanical stability and resistance against capillary forces were enhanced and allowed smaller pitch distances. This assumption is supported by the results obtained on the microscopic structures. Here, an elevated cross-linking density is in line with the reduced deformation and shrinkage found in structures developed by the improved procedure as shown in Fig. 4. Moreover, the homogeneous shrinkage obtained in structures upon post-curing indicates, that this method also reduces cross-linking inhomogeneities initially formed by the sequential laser exposure within the TPP-structures. An increased homogeneity of the polymer network results in less

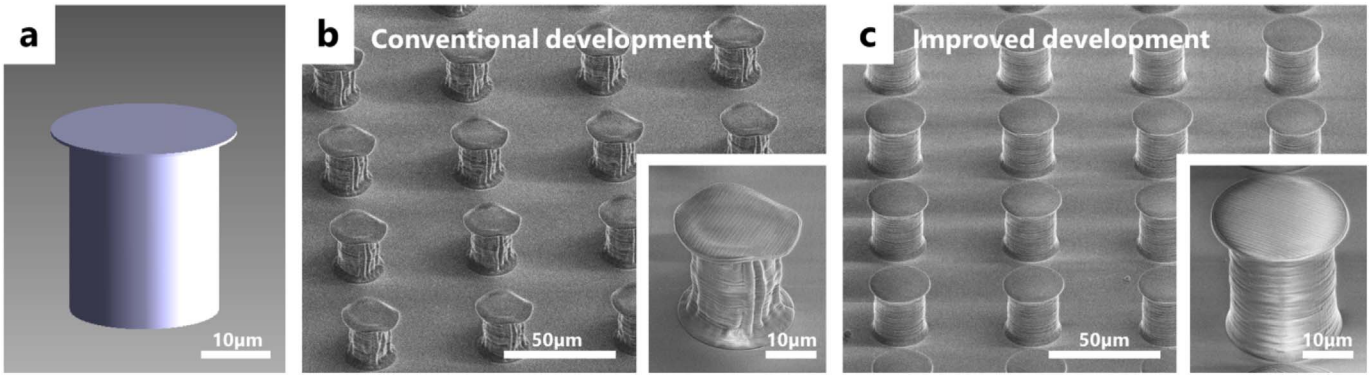

Fig. 4. Microscopic mushroom-shaped pillars. (a) 3d CAD-model of the mushroom-shaped pillar used for TPP. (b,c) Scanning electron micrographs at 50° tilt of structures developed either via (b) the conventional development or (c) the improved development strategy.

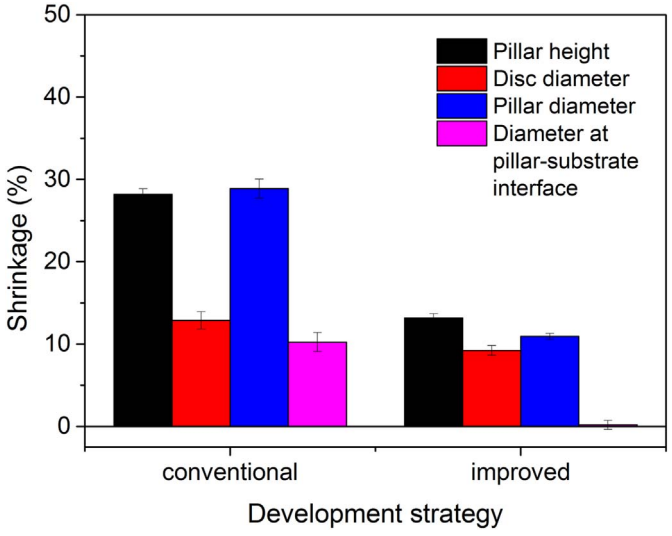

Fig. 5. Shrinkage of microscopic pillar structures. Pillar characteristics were extracted from SEM-images (n = 5) and compared to the original sizes used in the 3d CAD design.

internal stresses within the structures, and therefore, higher agreement with the original 3d model, as was observed.

The improved procedure can also be applied to accelerate the TPP fabrication process. A promising example is the fabrication of so-called core-shell structures. Here, only the shell (contour) of the structure and a few internal features supporting the shape of the shell are exposed and polymerized during the TPP, whereas a significant amount of the unreacted, liquid photo resist remains inside the structure. This approach can enormously speed up the process time, but requires a post UV cross-linking as presented in our paper; otherwise, the structures would suffer even more from shrinkage and capillary forces.

5. Conclusions

A novel development strategy for structures created by two-photon polymerization was introduced. The proposed approach enables a mechanical stabilization of created structures, before they are exposed to capillary forces. The feasibility of the improved method was demonstrated for densely packed nanopillar arrays and complex shaped microstructures, wherein the following conclusions can be drawn:

- The modified development procedure enables an additional UV-exposure before drying and, therefore, before exposing to capillary forces.
- A post UV-treatment of reactive groups, which remained unreacted upon the two-photon polymerization, enhances the cross-linking density, and therefore, the mechanical stability of structures and their resistance against mechanical deformations. Thus, the number of defects and collapsed structures in densely packed arrays can be drastically reduced.
- UV cross-linking reduces the polymer shrinkage from 30 to 10%. In

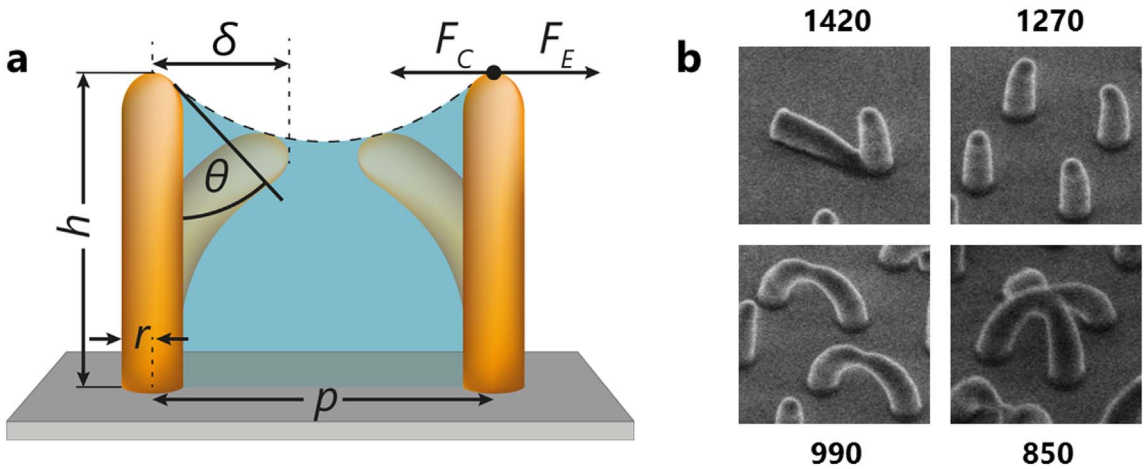

Fig. 6. Collapse of structures by capillary forces. (a) Schematic illustration of forces acting on pillars during evaporation. The ratio between the capillary force (F_C) and elastic restoring force (F_E) determines the type of collapse. The forces depend mainly on the pillar height, h, radius of the pillars, r, receding contact angle θ, deflection of the pillar, δ, and pitch distance, p. (b) Different types of pillar collapse obtained for commonly developed structures as a function of pitch distance: ground collapse (p = 1420 nm), upright pillars with bent tips (p = 1270 nm), pairs of attached pillars (p = 990 nm) and clusters of more than two pillars ($p \leq$ 850 nm).

addition, the shrinkage is almost isotropic compared to the anisotropic shrinkage of not post-treated structures.

Supplementary data to this article can be found online at https://doi.org/10.1016/j.mee.2018.03.009.

Acknowledgements

The authors gratefully acknowledge valuable input by Stefanie Faust; the reported findings about gecko-inspired structures were obtained within her bachelor thesis project. In addition, we thank Reza Hosseinabadi for his help with the TPP-fabrication. R.H. acknowledges partial funding from the European Research Council under the European Union's Seventh Framework Program (FP/2007-2013)/ERC Advanced Grant no. 340929.

References

[1] M. Farsari, B.N. Chichkov, Materials processing: two-photon fabrication, Nat. Photonics 3 (8) (2009) 450–452.
[2] G. von Freymann, A. Ledermann, M. Thiel, I. Staude, S. Essig, K. Busch, M. Wegener, Three-dimensional nanostructures for photonics, Adv. Funct. Mater. 20 (7) (2010) 1038–1052.
[3] S. Thiele, K. Arzenbacher, T. Gissibl, H. Giessen, A.M. Herkommer, 3D-printed eagle eye: compound microlens system for foveated imaging, Sci. Adv. 3 (2) (2017).
[4] S. Waheed, J.M. Cabot, N.P. Macdonald, T. Lewis, R.M. Guijt, B. Paull, M.C. Breadmore, 3D printed microfluidic devices: enablers and barriers, Lab Chip 16 (11) (2016) 1993–2013.
[5] A. Marino, C. Filippeschi, V. Mattoli, B. Mazzolai, G. Ciofani, Biomimicry at the nanoscale: current research and perspectives of two-photon polymerization, Nano 7 (7) (2015) 2841–2850.
[6] X. Zheng, W. Smith, J. Jackson, B. Moran, H. Cui, D. Chen, J. Ye, N. Fang, N. Rodriguez, T. Weisgraber, C.M. Spadaccini, Multiscale metallic metamaterials, Nat. Mater. 15 (10) (2016) 1100–1106.
[7] L.R. Meza, S. Das, J.R. Greer, Strong, lightweight, and recoverable three-dimensional ceramic nanolattices, Science 345 (6202) (2014) 1322–1326.
[8] J.K. Hohmann, M. Renner, E.H. Waller, G. von Freymann, Three-dimensional μ-printing: an enabling technology, Adv. Opt. Mater. 3 (11) (2015) 1488–1507.
[9] J.B. Mueller, J. Fischer, F. Mayer, M. Kadic, M. Wegener, Polymerization kinetics in three-dimensional direct laser writing, Adv. Mater. 26 (38) (2014) 6566–6571.
[10] X. Zhou, Y. Hou, J. Lin, A review on the processing accuracy of two-photon polymerization, AIP Adv. 5 (3) (2015) 030701.
[11] C. LaFratta, T. Baldacchini, Two-photon polymerization metrology: characterization methods of mechanisms and microstructures, Micromachines 8 (4) (2017) 101.
[12] P. Roca-Cusachs, F. Rico, E. Martínez, J. Toset, R. Farré, D. Navajas, Stability of microfabricated high aspect ratio structures in poly(dimethylsiloxane), Langmuir 21 (12) (2005) 5542–5548.
[13] K. Takada, K. Kaneko, Y.-D. Li, S. Kawata, Q.-D. Chen, H.-B. Sun, Temperature effects on pinpoint photopolymerization and polymerized micronanostructures, Appl. Phys. Lett. 92 (4) (2008) 041902.
[14] H.-B. Sun, T. Suwa, K. Takada, R.P. Zaccaria, M.-S. Kim, K.-S. Lee, S. Kawata, Shape precompensation in two-photon laser nanowriting of photonic lattices, Appl. Phys. Lett. 85 (17) (2004) 3708–3710.
[15] T.W. Lim, Y. Son, D.-Y. Yang, T.A. Pham, D.-P. Kim, B.-I. Yang, K.-S. Lee, S.H. Park, Net shape manufacturing of three-dimensional SiCN ceramic microstructures using an isotropic shrinkage method by introducing shrinkage guiders, Int. J. Appl. Ceram. Technol. 5 (3) (2008) 258–264.
[16] S.-H. Park, K.H. Kim, T.W. Lim, D.-Y. Yang, K.-S. Lee, Investigation of three-dimensional pattern collapse owing to surface tension using an imperfection finite element model, Microelectron. Eng. 85 (2) (2008) 432–439.
[17] D.F. Bray, J. Bagu, P. Koegler, Comparison of hexamethyldisilazane (HMDS), Peldri II, and critical-point drying methods for scanning electron microscopy of biological specimens, Microsc. Res. Tech. 26 (6) (1993) 489–495.
[18] N.H. Hazrin-Chong, M. Manefield, An alternative SEM drying method using hexamethyldisilazane (HMDS) for microbial cell attachment studies on sub-bituminous coal, J. Microbiol. Methods 90 (2) (2012) 96–99.
[19] H. Namatsu, K. Kurihara, M. Nagase, K. Iwadate, K. Murase, Dimensional limitations of silicon nanolines resulting from pattern distortion due to surface tension of rinse water, Appl. Phys. Lett. 66 (20) (1995) 2655–2657.
[20] H. Namatsu, K. Yamazaki, K. Kurihara, Supercritical drying for nanostructure fabrication without pattern collapse, Microelectron. Eng. 46 (1) (1999) 129–132.
[21] P.B. Clapham, M.C. Hutley, Reduction of lens reflexion by the moth eye principle, Nature 244 (5414) (1973) 281–282.
[22] S.J. Wilson, M.C. Hutley, The optical properties of 'Moth Eye' antireflection surfaces, Opt. Acta 29 (7) (1982) 993–1009.
[23] W.-L. Min, B. Jiang, P. Jiang, Bioinspired self-cleaning antireflection coatings, Adv. Mater. 20 (20) (2008) 3914–3918.
[24] A. del Campo, C. Greiner, E. Arzt, Contact shape controls adhesion of bioinspired fibrillar surfaces, Langmuir 23 (20) (2007) 10235–10243.
[25] D. Chandra, S. Yang, Capillary-force-induced clustering of micropillar arrays: is it caused by isolated capillary bridges or by the lateral capillary meniscus interaction force? Langmuir 25 (18) (2009) 10430–10434.
[26] A. Finn, R. Hensel, F. Hagemann, R. Kirchner, A. Jahn, W.-J. Fischer, Geometrical properties of multilayer nano-imprint-lithography molds for optical applications, Microelectron. Eng. 98 (Supplement C) (2012) 284–287.
[27] D. Chandra, S. Yang, Stability of high-aspect-ratio micropillar arrays against adhesive and capillary forces, Acc. Chem. Res. 43 (8) (2010) 1080–1091.
[28] B. Pokroy, S.H. Kang, L. Mahadevan, J. Aizenberg, Self-organization of a mesoscale bristle into ordered, hierarchical helical assemblies, Science 323 (5911) (2009) 237–240.
[29] Y. Hu, Z. Lao, B.P. Cumming, D. Wu, J. Li, H. Liang, J. Chu, W. Huang, M. Gu, Laser printing hierarchical structures with the aid of controlled capillary-driven self-assembly, Proc. Natl. Acad. Sci. 112 (22) (2015) 6876–6881.